

Probing the nature of the Higgs-gluon coupling

Robert V. Harlander* and Tobias Neumann†

Bergische Universität Wuppertal, 42097 Wuppertal, Germany

One and two-jet observables of dimension-7 Higgs-gluon coupling operators are studied as probes of possible deviations from the top-loop induced gluon-Higgs coupling. We discuss the case of both a scalar as well as a pseudo-scalar Higgs boson and show that higher order operators can give visible deviations from SM distribution shapes.

I. INTRODUCTION

The mechanism of electroweak symmetry breaking (EWSB) is in its phase of identification. The recent discovery [1, 2] of a Higgs boson at the Large Hadron Collider (LHC) provides a new probe for physics beyond the Standard Model (SM) through precision physics. Up to now, the signals are in very good agreement with SM predictions, but there is still room for traces of an extended theory.

The production and decay rates of the SM Higgs boson have been predicted by higher order theoretical calculations (see Refs. [3–5]). The dominant production mechanism is through gluon fusion, where the coupling of the gluons to the Higgs boson is mediated predominantly by a top-quark loop. It should be one of prior goals of the LHC to test the character of this gluon-Higgs coupling.

The loop-induced coupling differs particularly strongly from a point-like coupling if an external mass scale of the process becomes larger than the top-quark mass, and thus allows to resolve the non-trivial structure of the Higgs-gluon vertex. This suggests to look at processes involving large transverse momenta of the Higgs boson or an associated jet, for example, and compare the SM prediction with a point-like coupling.

A general description of a point-like gluon-Higgs coupling that is compatible with the gauge symmetries of the SM can be obtained in terms of an effective theory. The leading operator for a scalar Higgs, $\mathcal{O}_1 = H F_{\mu\nu}^a F^{a,\mu\nu}$ is of mass dimension 5. In the limit of infinite top mass, $m_t \rightarrow \infty$, and neglecting the Yukawa coupling of lighter quarks, the SM gluon-Higgs coupling reduces to this single operator; for finite m_t , it allows for a reasonable approximation of the SM gluon-Higgs coupling and is typically used for evaluating perturbative correction factors to the SM cross section prediction. Differential cross sections based on \mathcal{O}_1 have therefore been studied quite extensively. The purpose of our paper is to see the effect of higher dimensional operators on the most important kinematical distributions. These operators of mass dimension 7 are well known; they will be recalled in the next section.

The philosophy of our analysis is thus as follows: assume that it turns out that the gluon-Higgs coupling is *not* (or not mainly) induced by a top-quark loop as in the SM, but by point-like vertices generated by some new physics at higher scale. The coupling strengths of the effective operators (at least one of them) has to be SM-like in order to account for the signal strength observed experimentally. It will then be important to carefully consider distributions and compare them with the predictions based on the effective Lagrangian to be introduced below. Our discussion includes both the production of scalar and pseudo-scalar Higgs bosons (both denoted as H in what follows) and will be based on $H+1$ - and $H+2$ -jet observables.

Before we begin our discussion, let us first list some complementary approaches to quantify deviations from SM EWSB:

- The “LHCHSWG interim recommendations to explore the coupling structure of a Higgs-Like particle” [6] assume a single SM Higgs-like state H at roughly 125 GeV and look at its production and decay through $(\sigma \cdot \text{BR})(ii \rightarrow H \rightarrow ff) = \sigma_{ii} \Gamma_{ff} / \Gamma_H$, where ii and ff name the initial and final state configurations. They take SM deviations into account by modifying strengths of SM operators but keeping the same tensor structure.

*Electronic address: robert.harlander@uni-wuppertal.de

†Electronic address: tobias.neumann@uni-wuppertal.de

- The SILH effective model [7] corresponds to an effective theory for SM fields plus a Higgs-like particle. The leading QCD operator for Higgs production in SILH is just $H F_{\mu\nu}^a F^{a\mu\nu}$, which is also included in our analysis, of course.
- The approach in [8] takes BSM physics into account by the most general set of dimension-5 operators consistent with symmetries and therefore augments the “LHCHSWG recommendation” [6]. It can parametrize less SM-like physics and possibly include SILH physics.

Note that none of these approaches takes higher dimensional gluonic operators into account, which is the subject of this paper. Our motivation is that the dominant Higgs production mechanism at the LHC is gluon fusion, and we want to study the sensitivity of kinematical distributions of the Higgs boson and the associated jets to the precise form of the Higgs-gluon coupling. For similar, though more model-specific analyses, see Refs. [9–12], for example.

The remainder of this paper is organized as follows. In section II, the basis of dimension-5 and -7 operators is recalled that couple a scalar or a pseudo-scalar particle to gluons in a gauge invariant way. We also briefly describe some technical issues of our study. Section III presents distributions of $H+1$ -jet and $H+2$ -jets observables as induced by the formally leading and sub-leading terms in the effective theory. The SM case is reproduced for comparison. In section IV, we also consider terms that are formally suppressed by higher powers of the “new physics scale” Λ which occurs in the effective theory. In Section V we present our conclusions.

II. BASIS OF DIMENSION-7 OPERATORS AND THEIR IMPLEMENTATION

This section describes the operator basis used in our calculation. We start with the effective Lagrangian for the coupling of a scalar boson to gluons, and generalize the discussion to pseudo-scalar bosons in the subsequent section.

A. Scalar Higgs boson

The effective Lagrangian involving operators through mass dimension 7 which couple a scalar Higgs boson H to gluons can be written as [13, 14] (see also Ref. [15])

$$\mathcal{L} = \frac{C_1}{\Lambda} \mathcal{O}_1 + \sum_{n=2}^5 \frac{C_n}{\Lambda^3} \mathcal{O}_n \quad (1)$$

$$\begin{aligned} \mathcal{O}_1 &= H F_{\mu\nu}^a F^{a\mu\nu}, \quad \mathcal{O}_2 = H D_\alpha F_{\mu\nu}^a D^\alpha F^{a\mu\nu}, \quad \mathcal{O}_3 = H F_\nu^{a\mu} F_\sigma^{b\nu} F_\mu^{c\sigma} f^{abc}, \\ \mathcal{O}_4 &= H D^\alpha F_{\alpha\nu}^a D_\beta F^{a\beta\nu}, \quad \mathcal{O}_5 = H F_{\alpha\nu}^a D^\nu D^\beta F_\beta^{a\alpha}, \end{aligned} \quad (2)$$

where

$$F_{\mu\nu}^a = \partial_\mu A_\nu^a - \partial_\nu A_\mu^a - g_s f^{abc} A_\mu^b A_\nu^c, \quad D_\mu A_\nu^a = \partial_\mu A_\nu^a - g_s f^{abc} A_\mu^b A_\nu^c, \quad (3)$$

with the gluon field A_μ^a . The strong coupling is denoted by g_s , and f^{abc} are the SU(3) structure constants. We remark that, for an on-shell Higgs boson, the operators in Eq. (2) are not linearly independent. Instead, one finds $m_H^2 \mathcal{O}_1 = 4\mathcal{O}_5 - 2\mathcal{O}_2 + 4g_s \mathcal{O}_3$, where m_H is the Higgs mass, and thus one of \mathcal{O}_2 , \mathcal{O}_3 , and \mathcal{O}_5 could be eliminated from our analysis. Nevertheless, we find the basis in Eq. (2) convenient and therefore stick to this redundancy.

The mass parameter Λ in Eq. (1) is undetermined *a priori*; in the SM, it is the top-quark mass m_t , for example. Matching the effective Lagrangian of Eq. (1) to the SM allows one to derive perturbative expressions C_i^{SM} for the Wilson coefficients C_i . For example, C_1^{SM} is known through N⁴LO [16, 17]; explicit expressions for the C_n^{SM} ($n \in \{2, \dots, 5\}$),

on the other hand, have been obtained only at NLO [14], where we give the LO expressions as follows:¹

$$\begin{aligned}
C_1^{\text{SM}} &= \frac{g_s^2 \lambda_t}{48\pi^2} + \mathcal{O}(g_s^4) \simeq 2.2 \cdot 10^{-3}, \\
C_2^{\text{SM}} &= \frac{-7g_s^2 \lambda_t}{2880\pi^2} + \mathcal{O}(g_s^4) \simeq -2.6 \cdot 10^{-4}, \\
C_3^{\text{SM}} &= -\frac{g_s^3 \lambda_t}{240\pi^2} + \mathcal{O}(g_s^5) \simeq -5.3 \cdot 10^{-4}, \\
C_4^{\text{SM}} &= \frac{g_s^2 \lambda_t}{1440\pi^2} + \mathcal{O}(g_s^4) \simeq 7.3 \cdot 10^{-5}, \\
C_5^{\text{SM}} &= \frac{g_s^2 \lambda_t}{80\pi^2} + \mathcal{O}(g_s^4) \simeq 1.3 \cdot 10^{-3},
\end{aligned} \tag{4}$$

where $\lambda_t = m_t/v$ is the top-quark Yukawa coupling, and the values $m_t = 172 \text{ GeV}$, $v = 246 \text{ GeV}$, and $g_s = \sqrt{4\pi\alpha_s}$, with $\alpha_s = 0.118$ have been inserted in order to arrive at a numerical illustration for the size of these coefficients.

Nominally, contributions of \mathcal{O}_1 are suppressed by $1/\Lambda^2$ in physical quantities, mixed terms of \mathcal{O}_1 with \mathcal{O}_2 to \mathcal{O}_5 are suppressed by $1/\Lambda^4$, etc. Note, however, that in the SM, the matching coefficients are proportional to $\lambda_t \sim m_t/v = \Lambda/v$. This cancels the pre-factor $1/\Lambda$ in Eq. (1) and thus the overall suppression. Since we want to keep the discussion as general as possible, we will mostly ignore the suppression of the higher dimensional operators; all that is relevant to us is the influence of the individual operators on the shape of the distributions.

a. Remark on operators containing quark fields. The operators \mathcal{O}_4 and \mathcal{O}_5 can be rewritten to operators containing two and one quark bilinears according to the QCD equations of motion [18–20]:

$$D^\mu F_{\mu\nu}^a(x) = g_s \bar{\Psi}(x) \gamma_\nu t^a \Psi(x). \tag{5}$$

In case of gluodynamics, these two operators then vanish [13]. They only contribute when their corresponding quark-representation can occur in the given process/Feynman diagrams.

B. Pseudo-Scalar operators

In addition to the production of a scalar Higgs boson, we also consider the pseudo-scalar analogue which, for the sake of simplicity, we also denote by H in this paper.² The corresponding effective operators are obtained from the scalar case by replacing one of the field strength tensors by its dual $\tilde{F}_{\mu\nu}^a = \frac{1}{2}\epsilon_{\mu\nu\rho\sigma}F^{a\rho\sigma}$, with the Levi-Civita symbol $\epsilon_{\mu\nu\rho\sigma}$. We therefore obtain

$$\mathcal{L} = \frac{\tilde{C}_1}{\Lambda} \mathcal{O}_1 + \sum_{n=2}^5 \frac{\tilde{C}_n}{\Lambda^3} \mathcal{O}_n, \tag{6}$$

$$\begin{aligned}
\tilde{\mathcal{O}}_1 &= H \tilde{F}_{\mu\nu}^a F^{a\mu\nu}, \quad \tilde{\mathcal{O}}_2 = H D_\alpha \tilde{F}_{\mu\nu}^a D^\alpha F^{a\mu\nu}, \quad \tilde{\mathcal{O}}_3 = H \tilde{F}_\nu^{a\mu} F_\sigma^{b\nu} F_\mu^{c\sigma} f^{abc}, \\
\tilde{\mathcal{O}}_4 &= H D^\alpha \tilde{F}_{\alpha\nu}^a D_\beta F^{a\beta\nu}, \quad \tilde{\mathcal{O}}_5 = H \tilde{F}_{\alpha\nu}^a D^\nu D^\beta F_\beta^{a\alpha}.
\end{aligned} \tag{7}$$

We generated the Feynman rules for the operators \mathcal{O}_n and $\tilde{\mathcal{O}}_n$ ($n = 1, \dots, 5$) using LanHEP [21] and confirmed their validity with FeynRules [22]. A non-zero contribution of the operator $\tilde{\mathcal{O}}_4$ involves at least six gluons; therefore, it does not appear in our numerical analysis below. Furthermore, similar to the scalar case, the remaining operators are not linearly independent for an on-shell Higgs boson, but for convenience we will include all of them in our analysis.

With the obtained vertices, the necessary LO Feynman graphs for $H+1$ -jet and $H+2$ -jets amplitudes were generated with DIANA [23] as FORM [24] code. The analytical expressions for the matrix elements were then calculated by

¹ Ref. [14] misses a factor of $-3/4$ in C_3^{SM} , at least at LO, which we correct here.

² It should be clear from the context whether H denotes the scalar or the pseudo-scalar Higgs boson.

inserting the Feynman rules, where we used Feynman gauge and Faddeev-Popov ghosts, as well as an axial gauge for cross checking. The calculation of the cross sections was performed by means of standard VEGAS integration.

The operator $\tilde{\mathcal{O}}_4$ only contributes at higher order or at 3-jet production. This can easily be seen by switching to the quark representation using QCD equations of motion. The only non-vanishing Feynman-vertex contribution contains three gluons and a quark-antiquark pair, thus it does not appear in the quantities considered in this paper at LO. All lower order vertices vanish due to the contraction of equal-momentum vectors with the Levi-Civita symbol.

III. KINEMATICAL DISTRIBUTIONS

In what follows, we consider the transverse momentum distribution of the Higgs-boson when it is produced in association with one or two jets, $H+1$ -jet and $H+2$ -jet for short. In the $H+1$ -jet case, we compare the distributions obtained for the point-like vertices \mathcal{O}_n and $\tilde{\mathcal{O}}_n$ ($n = 1, \dots, 5$) with the SM-like loop-induced coupling.

The differential cross section based on the Lagrangian of Eq. (1) can be written as

$$d\sigma = \sum_{i,j=1}^5 d\sigma_{ij}, \quad (8)$$

where $d\sigma_{ij}$ is due to terms of the form $\mathcal{O}_i \mathcal{O}_j^\dagger$. In order to be independent of the actual size of the Wilson coefficients, we consider kinematical distributions normalized to their respective contribution to the inclusive cross section σ_{ij} , i.e., $d\sigma_{ij}/\sigma_{ij}$. Absolute effects on the distributions within a given model, i.e., for concrete values of the Wilson coefficients C_i and the “new physics scale” Λ , can be derived by combining these normalized distributions with the numerical values for the total cross sections σ_{ij} provided in Appendix A. Notice that interference terms with $i \neq j$ need not be positive definite.

We will show distributions for LHC proton-proton collisions, split into the partonic gluon-gluon (gg), the gluon-quark (gq), and quark-quark (qq) initial states (qq includes quark-antiquark as well as different-flavor initial states). At LO, the operator \mathcal{O}_5 contributes only to the gq -channel because, according to Eq. (5), it can be rewritten to include a quark bilinear term. Analogously, \mathcal{O}_4 can be rewritten to contain two quark bilinears, and therefore only contributes to the qq channel. For the gq -channel, \mathcal{O}_3 does not contribute because its Feynman rules involve at least three gluons.

All distributions are generated for a Higgs mass of $m_H = 125$ GeV and a center of mass energy of $\sqrt{s} = 13$ TeV. For the $H+1$ -jet p_T -distributions, the choice of factorization and renormalization scale is $\mu = \sqrt{m_H^2 + p_T^2}$ and in case of $H+2$ -jet cross sections the jet- p_T geometric mean $\mu = \sqrt{p_T(j_1) p_T(j_2)}$. Due to our normalization, the results are largely unaffected by changes of m_H and \sqrt{s} .

A. $H+1$ -jet cross sections

First we consider the Higgs transverse momentum (p_T) distribution in $H+1$ -jet production for scalar and pseudo-scalar Higgs bosons in fig. 1 and 2. In both cases, one observes large differences in the p_T shape of the individual terms. For comparison, we show the curve which corresponds to SM-like Higgs production through a top-loop, obtained from the program **SusHi** [25] (curves denoted “SM” for the scalar and “top-loop” for the pseudo-scalar). Note, however, that strictly speaking the latter receives an additional p_T dependence through its proportionality to $\alpha_s^2(\mu)$, with $\mu = \sqrt{m_H^2 + p_T^2}$. In order to properly compare to the predictions from the effective theory, we have divided the SM and top-loop distribution by this factor.

The panel named “sum” in fig. 1 and 2 shows the sum over the partonic channels for fixed ij . The respective inclusive cross sections to which these curves are normalized are listed in table I and table II.

As a check, we used these results and combined them with the SM Wilson coefficients of Eq. (4) in order to reproduce the first two non-vanishing terms in the $1/m_t$ expansion for the p_T -distribution. The results are shown in fig. 3. They give some deeper insight into the observations of Ref. [26]. For the gg channel, the interference terms of \mathcal{O}_1 with the higher order operators have a very similar shape as the dominant $\mathcal{O}_1 \mathcal{O}_1^\dagger$ contribution. The effective theory approach to Higgs production in the SM therefore works extremely well for the gg subchannel, as observed also at NLO QCD in Ref. [26]. For the gq channel, on the other hand, the various contributions differ rather strongly among each other.

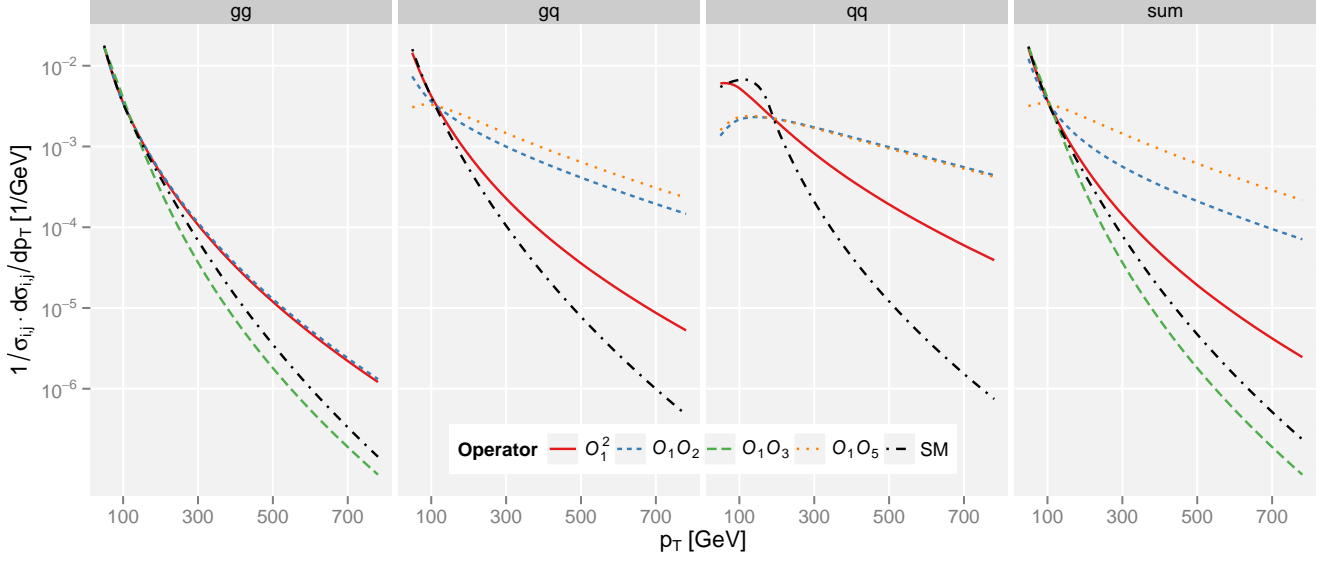


FIG. 1: Normalized Higgs transverse momentum distributions for scalar coupling operators. The normalization factors σ_{ij} are given in table I.

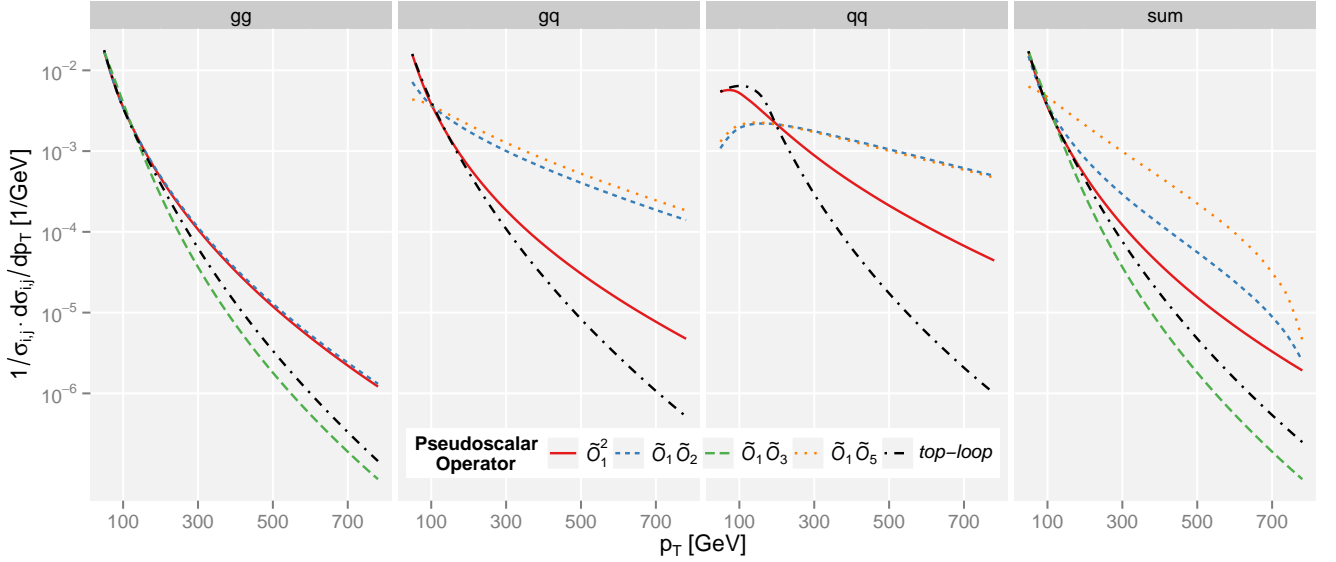


FIG. 2: Same as fig. 1, but for pseudo-scalar coupling operators. Note that the gg channel is identical to the scalar case. The σ_{ij} are given in table II.

The $\mathcal{O}_1 \mathcal{O}_5^\dagger$ term is even negative; since its magnitude hardly decreases towards larger p_T , it drives the gq channel to negative values. But note that, in contrast to fig. 1, the scale Λ enters these results, and that it is set to $\Lambda = m_t$; the higher dimensional operators therefore become numerically dominant at $p_T \gtrsim m_t$.

In contrast to the p_T distribution, we do not observe any significant differences for the rapidity distributions among the operators, which is why we refrain from showing these results here.



FIG. 3: Higgs transverse momentum distributions with SM matching coefficients, resulting in a total m_t^2 -suppression with respect to C_1^2 . Please note that in case of the gq and summed channel the crossterm $O_1 O_5$ has been multiplied with -1 . For the qq channel the crossterm $O_1 O_2$ has been multiplied with -1 .

B. Two jet cross sections

For two jets there are considerably more interesting observables than for the 1-jet case. In particular the azimuthal angle difference $\Delta\Phi_{jj}$ between the two jets and the rapidity separation $\Delta\eta_{jj}$ are well known 2-jet observables for gluon fusion and weak boson fusion (WBF) [27–30]. For example, suitable cuts in $\Delta\Phi_{jj}$ distributions allow one to discriminate a scalar from a pseudo-scalar Higgs boson in $H+2$ -jets production [31]. Also, $\Delta\Phi_{jj}$ and $\Delta\eta_{jj}$ have been proposed to distinguish $H+2$ -jet production through gluon fusion from WBF [28]. We will study these distributions for the higher dimensional operators of section II and see how they may affect the conclusions drawn from previous studies.

In the following we will use “inclusive” cuts for the $\Delta\eta_{jj}$ -distribution,

$$p_{j\perp} > 20 \text{ GeV}, \quad |\eta_j| < 5, \quad R_{jj} > 0.6, \quad (9)$$

where $R_{jj} = \sqrt{(\Delta\eta_{jj})^2 + (\Delta\Phi_{jj})^2}$, and additional “WBF cuts”

$$\Delta\eta_{jj} = |\eta_{j1} - \eta_{j2}| > 4.2, \quad \eta_{j1} \cdot \eta_{j2} < 0, \quad m_{jj} > 600 \text{ GeV} \quad (10)$$

for the $\Delta\Phi_{jj}$ distribution, where m_{jj} is the invariant mass of the two jets.

The $\Delta\Phi_{jj}$ distributions are shown in fig. 4 and fig. 5. The red curve, corresponding to the contribution from $O_1 O_1^\dagger$ ($\tilde{O}_1 \tilde{O}_1^\dagger$), reproduces the results of Ref. [31]. In the scalar as well as in the pseudo-scalar case the O_3 (\tilde{O}_3) induced term has a much stronger variation than the formally leading $O_1 O_1^\dagger$ and the interference terms $O_1 O_2^\dagger$ and $O_1 O_5^\dagger$ (respectively the corresponding pseudo-scalar terms). In the scalar case, the “4-quark-operator” O_4 leads to a remarkable deviation from the other terms. As before, “sum” refers to the sum over the partonic sub-channels for fixed ij .

Using `vbfn10` [32–34], we calculated the $\Delta\Phi_{jj}$ distributions for top-loop induced Higgs production. We find that they hardly differ from the results for $O_1^\dagger O_1$ (respectively $\tilde{O}_1^\dagger \tilde{O}_1$) and therefore refrain from including them in our plots.

An explanation for the different curvatures of the leading scalar and pseudo-scalar operators O_1 and \tilde{O}_1 , i.e. the suppression of planar events for CP-odd couplings, is that the epsilon tensor contracted with (four) linearly dependent momentum vectors of the incoming and outgoing partons vanishes [31].

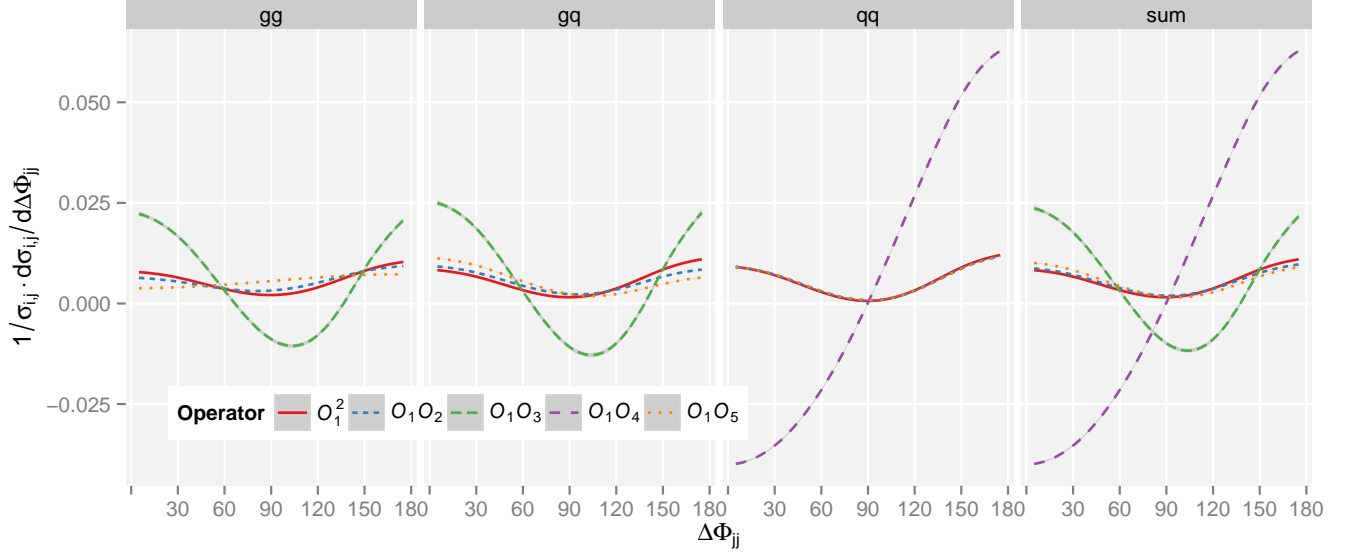


FIG. 4: Normalized distributions for azimuthal angle difference of the two final state jets for scalar operators. The σ_{ij} are given in table III.

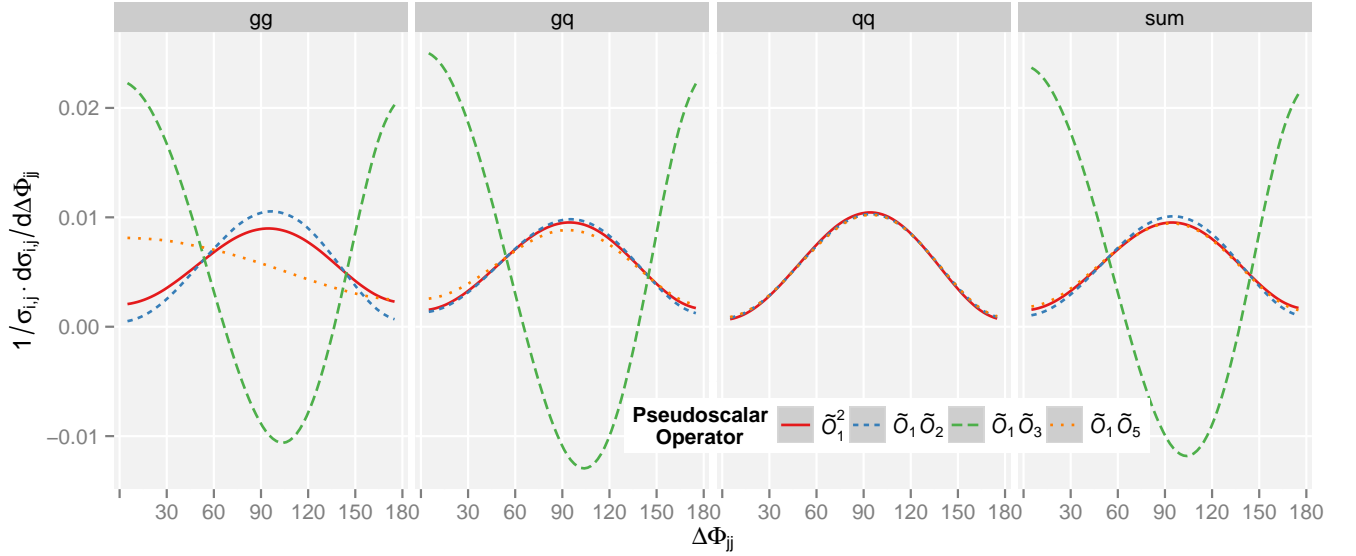


FIG. 5: Same as fig. 4, but for pseudo-scalar operators. The σ_{ij} are given in table IV.

In order to allow the reader to derive quantitative results for particular models corresponding to specific values for the Wilson coefficients, we provide again in table III and table IV the integrated cross sections derived with the inclusive plus WBF cuts described in Eqs. (9) and (10).

Distributions for the jet rapidity separation for scalar and pseudo-scalar operators are shown in fig. 6 and 7. The used normalization factors are given in table V and table VI. One can compare these with the results of [28, Figure 8], where the specifics for the $\Delta\eta_{jj}$ distribution for 2-jet gluon-fusion and 2-jet weak boson fusion are discussed: while gluon-fusion exhibits a peak at small $\Delta\eta_{jj}$ (due to the jet radius constraint $R_{jj} > 0.6$), for weak boson fusion the peak is at a rapidity separation $\Delta\eta_{jj} \approx 5$ and considerably smaller. We compared our results again to top-loop induced Higgs production obtained with `vbfnlo` [32–34]; similar to the $\Delta\Phi_{jj}$ distribution, we find that they are almost identical to the curves for $\mathcal{O}_1^\dagger \mathcal{O}_1$ (respectively $\tilde{\mathcal{O}}_1^\dagger \tilde{\mathcal{O}}_1$), which is why we refrain from including them in our plots.

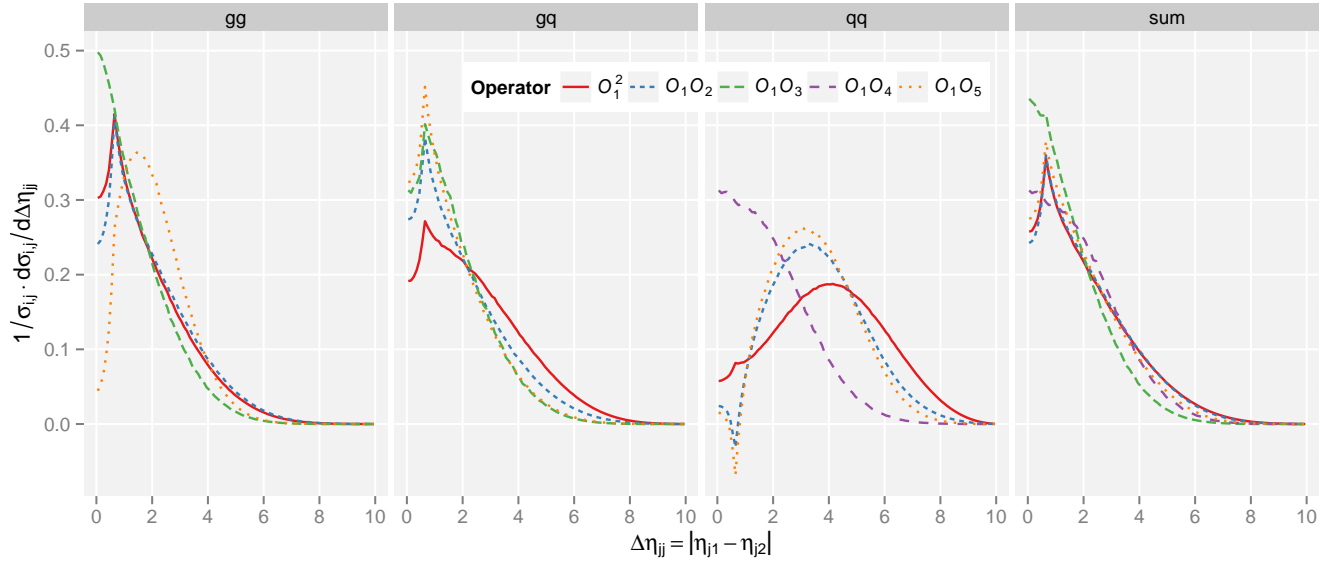


FIG. 6: Normalized distributions for rapidity separation of the two final state jets for scalar operators. The σ_{ij} are given in table V.

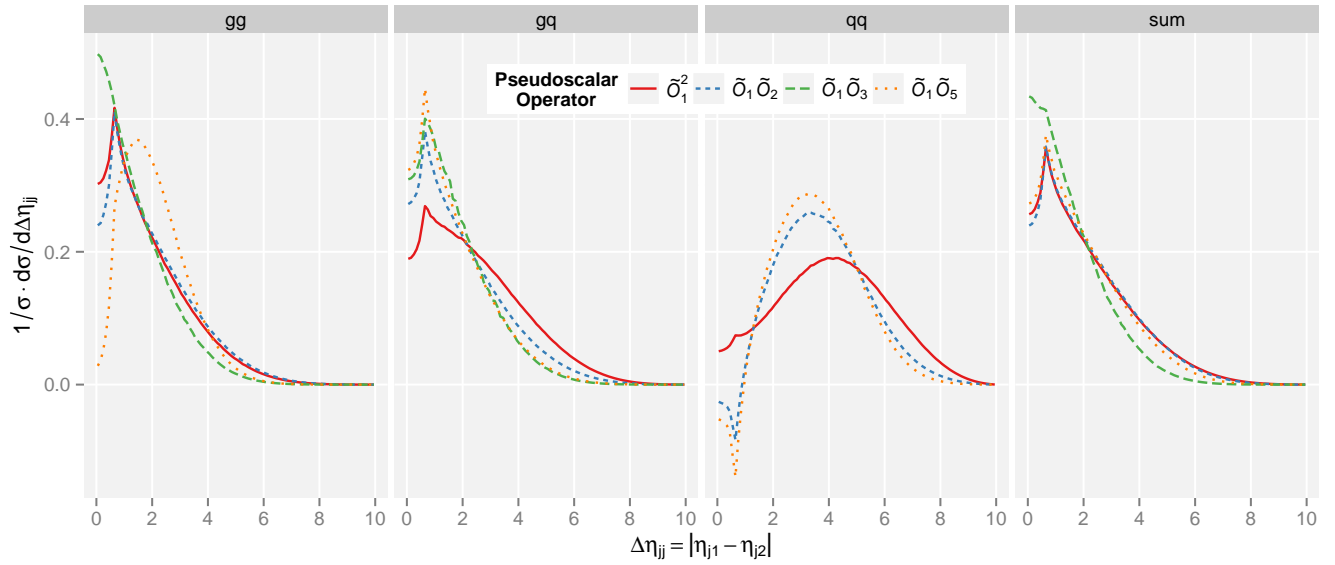


FIG. 7: Same as fig. 6, but for pseudo-scalar operators. The σ_{ij} are given in table VI.

While there are quantitative differences among the various contributions for the scalar and pseudo-scalar operators considered here, we conclude that the qualitative differences are probably too small to be used in an experimental analysis in order to classify the gluon-Higgs coupling.

In light of the fact that the differences among the various operators increase with the Higgs transverse momentum, see fig. 1 and 2, it is suggestive to consider the $\Delta\Phi_{jj}$ and $\Delta\eta_{jj}$ distributions for these high- p_T events only. For example, fig. 8 shows the result for the $\Delta\Phi_{jj}$ distribution in the scalar Higgs case, when the Higgs' transverse momentum is

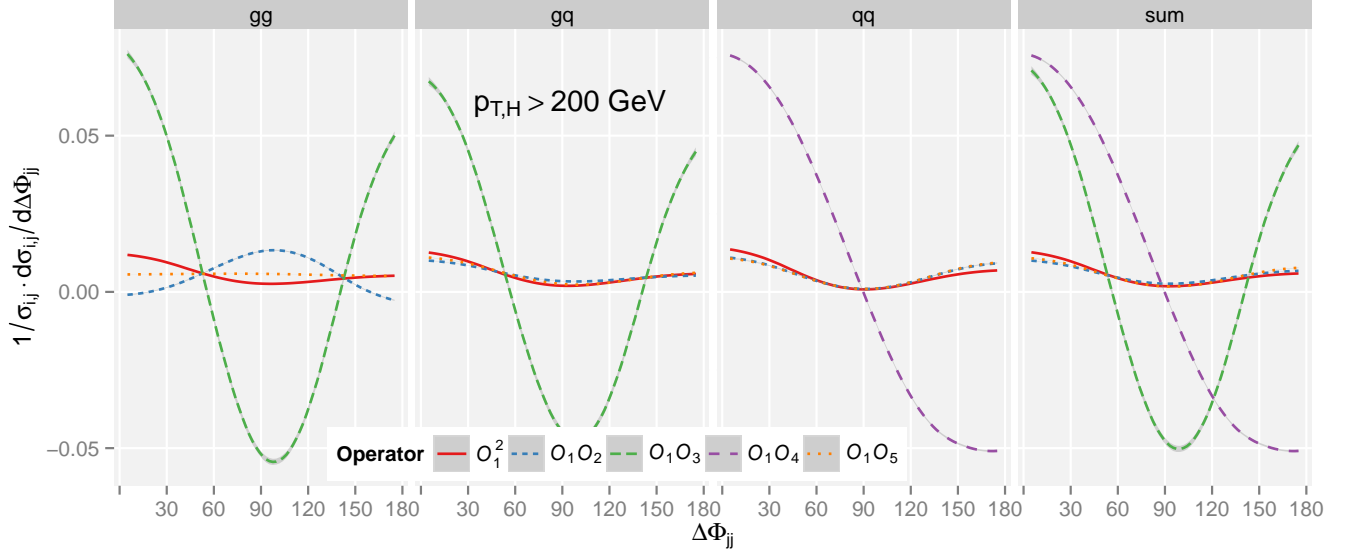


FIG. 8: Similar to fig. 4, but restricted to events with $p_T > 200$ GeV, where p_T is the transverse momentum of the Higgs boson. The σ_{ij} are given in table VII.

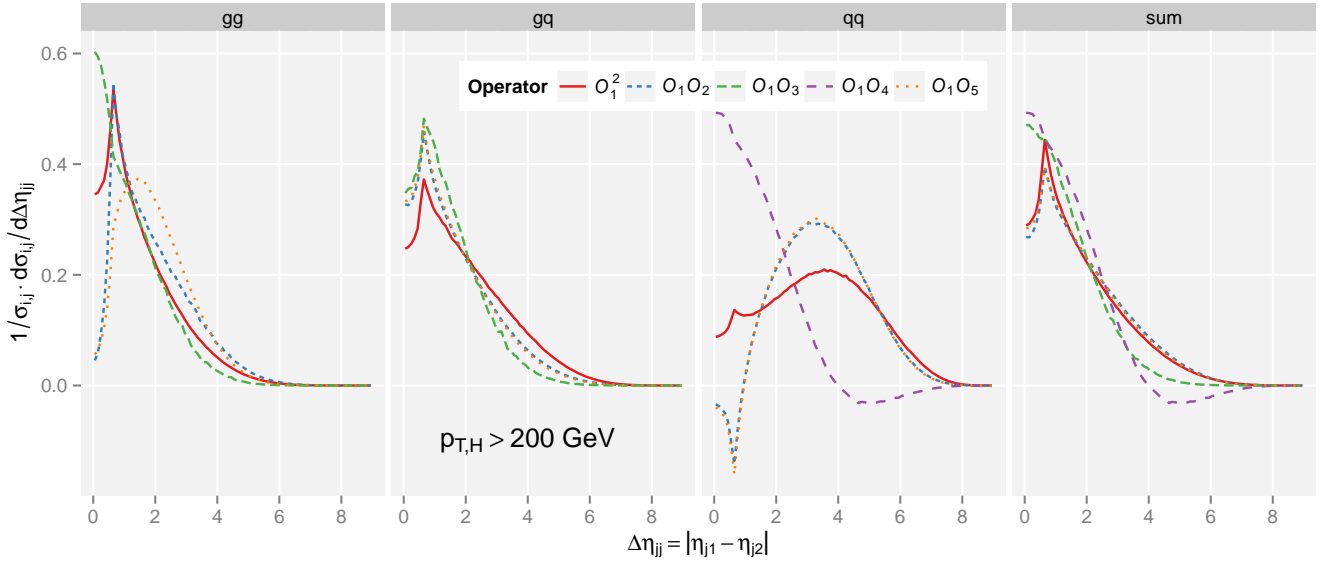


FIG. 9: Similar to fig. 6, but restricted to events with $p_T > 200$ GeV, where p_T is the transverse momentum of the Higgs boson. The σ_{ij} are given in table VIII.

restricted to $p_T > 200$ GeV. Compared to fig. 4, some of the features are strongly enhanced;³ however, considering the fact that such a cut will significantly decrease the data sample, it remains to be seen whether it would lead to an improvement of an experimental analysis.

³ The fact that the slope of “ $\mathcal{O}_1\mathcal{O}_4$ ” changes sign is due to a change of sign in the normalization, see table VII.

IV. HIGHER ORDER SUPPRESSED TERMS

Up to this point, we considered the Lagrangians in Eq.(1) and Eq.(6) as an effective theory truncated at $\mathcal{O}(1/\Lambda^3)$. Therefore, we only took into account the square of \mathcal{O}_1 (or $\tilde{\mathcal{O}}_1$) and its interference with \mathcal{O}_n (or $\tilde{\mathcal{O}}_n$) ($n \geq 2$), as other terms are of higher order in $1/\Lambda$. In this section, we will consider products of the \mathcal{O}_n (and $\tilde{\mathcal{O}}_n$) ($n \geq 2$) with each other. They might be relevant if indeed the gluon-Higgs coupling is predominantly mediated by one of the dimension-7 operators, as hypothesized in the introduction. This hypothesis is also the reason why we do not include interference terms of \mathcal{O}_1 with dimension-9 operators in this section, as it would be required if we were dealing with a regular analysis at fixed order in $1/\Lambda$.

FIG. 10 and 11 show the p_T -distributions in the $H+1$ -jet case as induced by the higher order operators. For comparison, we also include the formally leading term arising from $\mathcal{O}_1\mathcal{O}_1^\dagger$. Two observations in these figures are remarkable: on the one hand, the difference between the shapes of the higher order terms and this formally leading term is quite significant. On the other hand, the higher order terms themselves are all very close to each other. Also, the behavior is very similar in the scalar and the pseudo-scalar case.

The normalizations for the individual curves are given in table IX and X.

Similarly, we consider the $\Delta\Phi_{jj}$ distributions for the higher dimensional operators in fig. 12 and 13, and the $\Delta\eta_{jj}$ distributions in fig. 14 and 15. While there are quite large qualitative differences in the various $\Delta\Phi_{jj}$ distributions, they are far less prominent in the $\Delta\eta_{jj}$ shapes. The formally leading term induced by $\mathcal{O}_1\mathcal{O}_1^\dagger$ (and $\tilde{\mathcal{O}}_1\tilde{\mathcal{O}}_1^\dagger$) are again included for comparison.

The corresponding normalization factors are given in table XI, XII and table XIII, XIV.

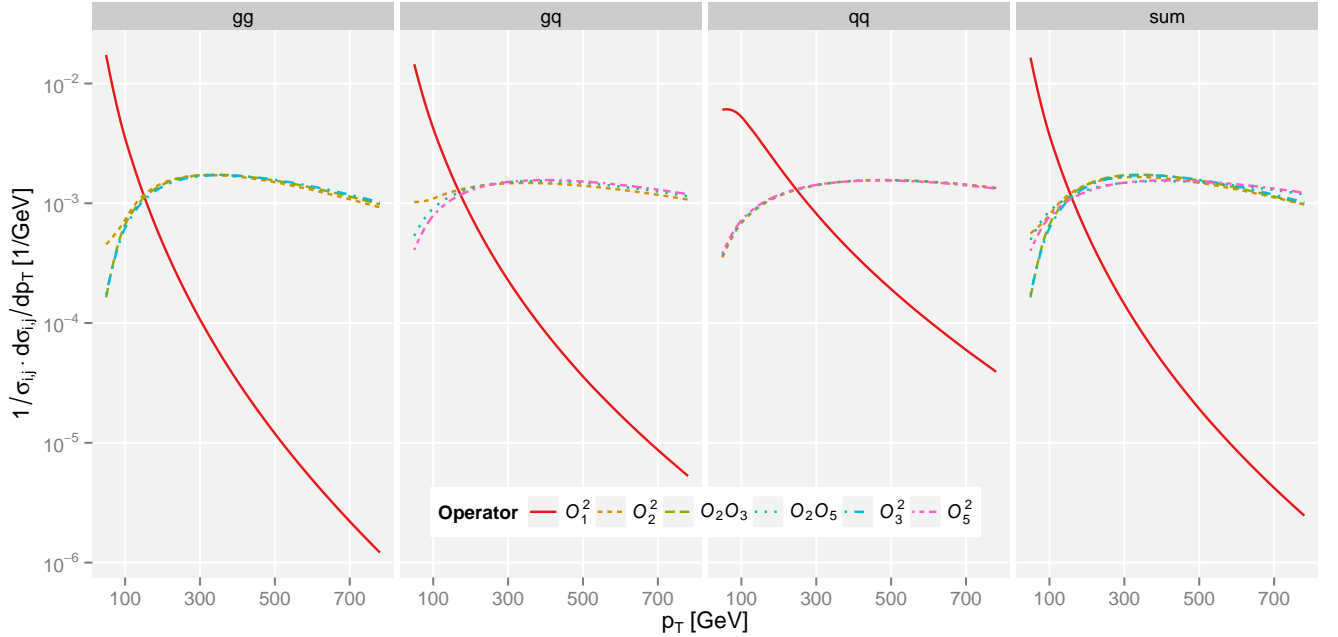


FIG. 10: Normalized Higgs transverse momentum distributions for scalar coupling operators. The σ_{ij} are given in table IX.

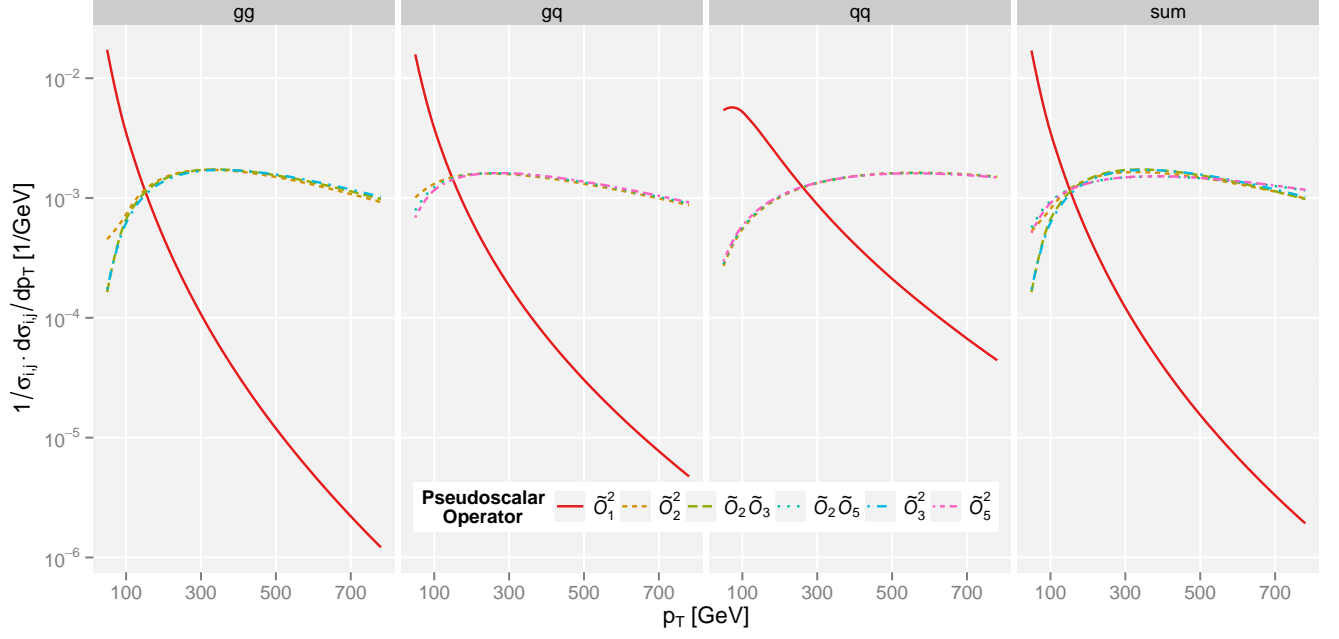


FIG. 11: Normalized Higgs transverse momentum distributions for pseudo-scalar coupling operators. Note that the gg channel is identical to the scalar case. The σ_{ij} are given in table X.

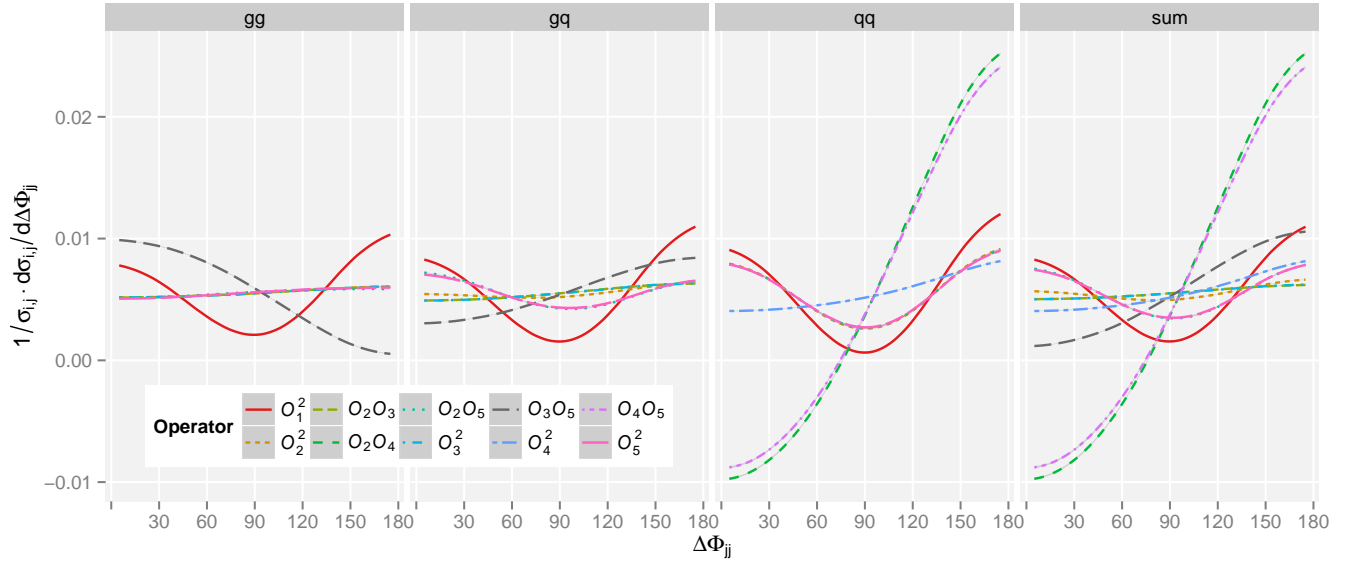


FIG. 12: Normalized distributions for azimuthal angle difference of the two final state jets for scalar operators. The σ_{ij} are given in table XI.

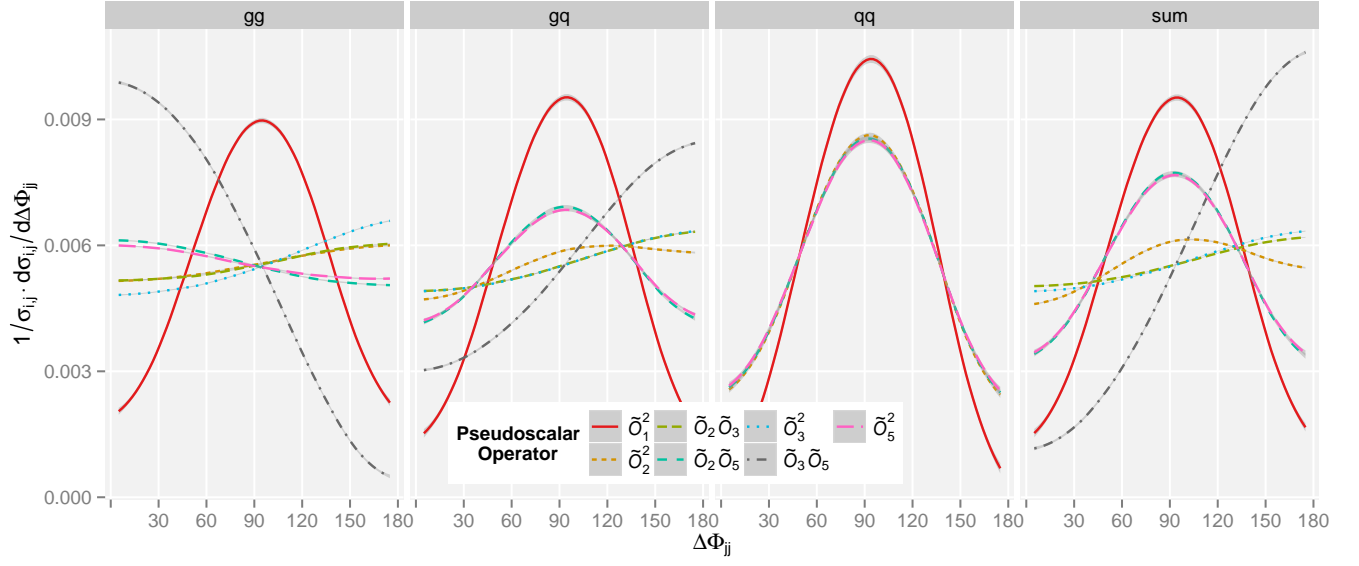


FIG. 13: Normalized distributions for azimuthal angle difference of the two final state jets for pseudo-scalar operators. The σ_{ij} are given in table XII.

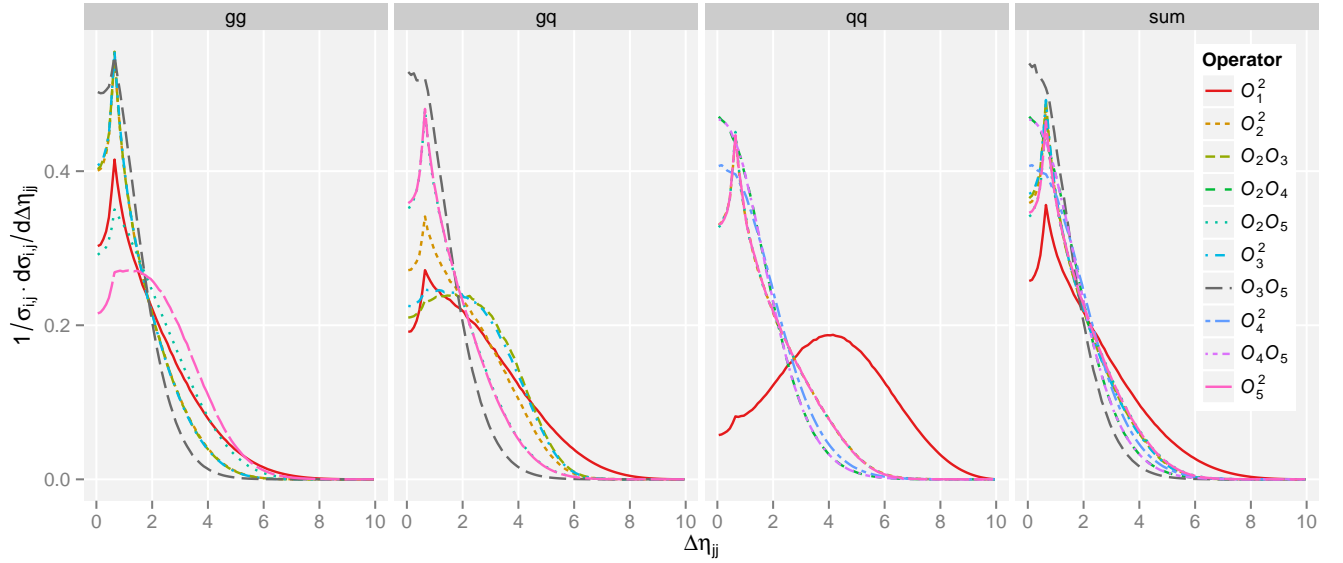


FIG. 14: Normalized distributions for rapidity separation of the two final state jets for scalar operators. The σ_{ij} are given in table XIII.

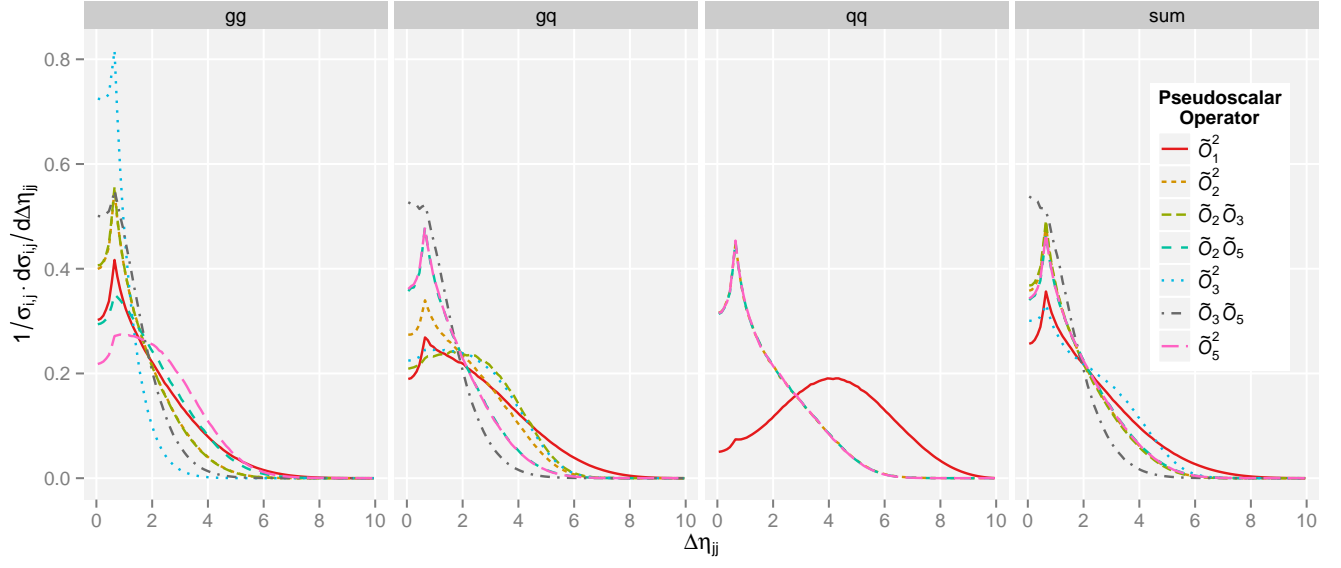


FIG. 15: Normalized distributions for rapidity separation of the two final state jets for pseudo-scalar operators. The σ_{ij} are given in table XIV.

V. CONCLUSIONS

In this paper we have studied the influence of higher dimensional operators that couple gluons to a scalar or a pseudo-scalar particle H on distributions in $H+1$ -jet and $H+2$ -jets production. While the SM assumes a (mostly) top-loop induced gluon-Higgs coupling, an analysis along the lines of our paper will be necessary in order to fully test this hypothesis. We have found that dimension-7 operators significantly affect the p_T distribution of the Higgs boson, leading to a much harder spectrum than in the SM. Also 2-jet observables can be quite sensitive to these effects that are formally subleading in the scale of “new physics”.

We note that since, to our knowledge, this is the first analysis of this kind, we have restricted ourselves to the lowest order of perturbation theory. If deviations in the observables discussed here relative to the SM prediction are observed, it will be necessary and interesting to perform this analysis at NLO QCD.

b. Acknowledgments We would like to thank D. Zeppenfeld for comments on the manuscript and calling our attention to Ref.[15] which considers the effect of dimension-7 operators to SM Higgs production. Further thanks go to H. Mantler for valuable help with the SM predictions. This work was supported by BMBF, contract 05H12PXE.

Appendix A: Normalization factors

In this appendix, we collect the normalization factors for the distributions calculated in this paper. They should allow the reader to reconstruct the absolute distributions for any particular model with specific values of the Wilson coefficients C_i or \tilde{C}_i , see Eqs.(1) and (6). Specifically, absolute cross sections $d\sigma_{ij}$ in picobarns are obtained by multiplying the numbers for $d\sigma_{ij}/\sigma_{ij}$ read off from the figures in Sections III and IV by the normalization factors σ_{ij} given in the tables below, times $\text{Re}(C_i^\dagger C_j)/(\Lambda/\text{GeV})^{(n_i+n_j)}$, where $n_1 = 1$ and $n_i = 3$ for $i \neq 1$.⁴ In other words, the numbers given here for the σ_{ij} refer to $\Lambda = 1 \text{ GeV}$ and $C_i = 1 \forall i$.

σ_{ij}/pb for $H+1$ -jet (scalar)			
ij	gg	gq	qq
SM/ α_s^2	$4.79 \cdot 10^2$	$1.78 \cdot 10^2$	3.13
11	$3.88 \cdot 10^{10}$	$1.59 \cdot 10^{10}$	$1.03 \cdot 10^8$
12	$-5.55 \cdot 10^{14}$	$-6.59 \cdot 10^{14}$	$3.05 \cdot 10^{13}$
13	$-2.00 \cdot 10^{13}$	—	—
15	—	$-2.05 \cdot 10^{14}$	$1.60 \cdot 10^{13}$

TABLE I: Normalization factors for p_T distributions in $H+1$ -jet production for a scalar Higgs. They are obtained by integrating the distributions of fig. 1 over the interval $p_T \in [30, 800] \text{ GeV}$.

σ_{ij}/pb for $H+1$ -jet (pseudo-scalar)			
ij	gg	gq	qq
top-loop/ α_s^2	$1.11 \cdot 10^3$	$4.16 \cdot 10^2$	6.67
11	$3.88 \cdot 10^{10}$	$5.06 \cdot 10^9$	$3.13 \cdot 10^8$
12	$-5.56 \cdot 10^{14}$	$-3.22 \cdot 10^{14}$	$8.87 \cdot 10^{13}$
13	$-2.00 \cdot 10^{13}$	—	—
15	—	$-1.21 \cdot 10^{14}$	$4.68 \cdot 10^{13}$

TABLE II: Same as table I, but for a pseudo-scalar Higgs (see fig. 2).

⁴ This factor is not required for the cross sections labelled “SM” or “top-loop”, of course.

σ_{ij}/pb for $H+2\text{-jet}$ (scalar), WBF cuts			
ij	gg	gq	qq
11	$1.43 \cdot 10^9$	$2.27 \cdot 10^9$	$8.42 \cdot 10^8$
12	$-2.14 \cdot 10^{13}$	$-6.54 \cdot 10^{13}$	$-4.47 \cdot 10^{13}$
13	$-7.13 \cdot 10^{11}$	$-7.59 \cdot 10^{11}$	—
14	—	—	$-1.19 \cdot 10^{12}$
15	$-4.65 \cdot 10^{11}$	$-1.60 \cdot 10^{13}$	$-1.58 \cdot 10^{13}$

TABLE III: Normalization factors for $\Delta\Phi_{jj}$ distributions in $H+2\text{-jets}$ production for a scalar Higgs. They are obtained by integrating the distributions of fig. 4 over the interval $\Delta\Phi_{jj} \in [0, \pi]$, with the cuts described in Eqs. (9) and (10).

σ_{ij}/pb for $H+2\text{-jet}$ (pseudo-scalar), WBF cuts			
ij	gg	gq	qq
11	$1.42 \cdot 10^9$	$2.24 \cdot 10^9$	$8.29 \cdot 10^8$
12	$-2.11 \cdot 10^{13}$	$-6.66 \cdot 10^{13}$	$-4.41 \cdot 10^{13}$
13	$-7.12 \cdot 10^{11}$	$-7.57 \cdot 10^{11}$	—
14	—	—	—
15	$-4.43 \cdot 10^{11}$	$-1.68 \cdot 10^{13}$	$-1.55 \cdot 10^{13}$

TABLE IV: Same as table III, but for a pseudo-scalar Higgs (see fig. 5).

σ_{ij}/pb for $H+2\text{-jet}$ (scalar), incl. cuts			
ij	gg	gq	qq
11	$5.00 \cdot 10^{10}$	$2.67 \cdot 10^{10}$	$2.50 \cdot 10^9$
12	$-6.41 \cdot 10^{14}$	$-1.05 \cdot 10^{15}$	$-1.48 \cdot 10^{14}$
13	$-6.11 \cdot 10^{13}$	$-3.11 \cdot 10^{13}$	—
14	—	—	$-1.71 \cdot 10^{13}$
15	$-1.42 \cdot 10^{13}$	$-3.59 \cdot 10^{14}$	$-5.51 \cdot 10^{13}$

TABLE V: Normalization factors for $\Delta\eta_{jj}$ distributions in $H+2\text{-jets}$ production for a scalar Higgs. They are obtained by integrating the distributions of fig. 6 over the interval $\Delta\eta_{jj} \in [0, 10]$, with the cuts described in Eqs. (9).

σ_{ij}/pb for $H+2\text{-jet}$ (pseudo-scalar), incl. cuts			
ij	gg	gq	qq
11	$4.94 \cdot 10^{10}$	$2.62 \cdot 10^{10}$	$2.39 \cdot 10^9$
12	$-6.32 \cdot 10^{14}$	$-1.07 \cdot 10^{15}$	$-1.31 \cdot 10^{14}$
13	$-6.11 \cdot 10^{13}$	$-3.11 \cdot 10^{13}$	—
14	—	—	—
15	$-1.36 \cdot 10^{13}$	$-3.70 \cdot 10^{14}$	$-4.74 \cdot 10^{13}$

TABLE VI: Same as table V, but for a pseudo-scalar Higgs (see fig. 7).

σ_{ij}/pb for $H+2\text{-jet}$ (scalar), WBF cuts $p_{T,H} > 200 \text{ GeV}$			
ij	gg	gq	qq
11	$1.14 \cdot 10^8$	$2.36 \cdot 10^8$	$1.23 \cdot 10^8$
12	$-1.91 \cdot 10^{12}$	$-2.32 \cdot 10^{13}$	$-2.25 \cdot 10^{13}$
13	$-1.28 \cdot 10^{11}$	$-1.93 \cdot 10^{11}$	—
14	—	—	$3.82 \cdot 10^{11}$
15	$-2.34 \cdot 10^{11}$	$-1.00 \cdot 10^{13}$	$-1.03 \cdot 10^{13}$

TABLE VII: Normalization factors for $\Delta\Phi_{jj}$ distributions in $H+2\text{-jets}$ production for a scalar Higgs with $p_T > 200 \text{ GeV}$. They are obtained by integrating the distributions of fig. 8 over the interval $\Delta\Phi_{jj} \in [0, \pi]$, with the cuts described in Eqs. (9) and (10).

σ_{ij}/pb for $H+2\text{-jet}$ (scalar), incl. cuts $p_{T,H} > 200 \text{ GeV}$			
ij	gg	gq	qq
11	$3.58 \cdot 10^9$	$2.95 \cdot 10^9$	$3.84 \cdot 10^8$
12	$-3.83 \cdot 10^{13}$	$-5.05 \cdot 10^{14}$	$-7.00 \cdot 10^{13}$
13	$-1.21 \cdot 10^{13}$	$-1.30 \cdot 10^{13}$	—
14	—	—	$-6.14 \cdot 10^{12}$
15	$-6.57 \cdot 10^{12}$	$-2.46 \cdot 10^{14}$	$-3.23 \cdot 10^{13}$

TABLE VIII: Normalization factors for $\Delta\eta_{jj}$ distributions in $H+2\text{-jets}$ production for a scalar Higgs with $p_T > 200 \text{ GeV}$. They are obtained by integrating the distributions of fig. 6 over the interval $\Delta\eta_{jj} \in [0, 10]$, with the cuts described in Eqs. (9).

σ_{ij}/pb for $H+1\text{-jet}$ (scalar)			
ij	gg	gq	qq
22	$1.35 \cdot 10^{20}$	$3.60 \cdot 10^{19}$	$1.00 \cdot 10^{19}$
23	$-1.12 \cdot 10^{20}$	—	—
25	—	$3.35 \cdot 10^{19}$	$1.01 \cdot 10^{19}$
33	$2.38 \cdot 10^{19}$	—	—
55	—	$7.97 \cdot 10^{18}$	$2.57 \cdot 10^{18}$

TABLE IX: Normalization factors for p_T distributions in $H+1\text{-jet}$ production induced by higher dimensional operators for a scalar Higgs (see fig. 10).

σ_{ij}/pb for $H+1\text{-jet}$ (pseudo-scalar)			
ij	gg	gq	qq
22	$1.35 \cdot 10^{20}$	$3.61 \cdot 10^{19}$	$2.67 \cdot 10^{19}$
23	$-1.12 \cdot 10^{20}$	—	—
25	—	$3.48 \cdot 10^{19}$	$2.71 \cdot 10^{19}$
33	$2.38 \cdot 10^{19}$	—	—
55	—	$8.47 \cdot 10^{18}$	$6.87 \cdot 10^{18}$

TABLE X: Same as table IX, but for a pseudo-scalar Higgs (see fig. 11).

σ_{ij}/pb for $H+2\text{-jet}$ (scalar), WBF cuts			
ij	gg	gq	qq
22	$1.40 \cdot 10^{19}$	$2.01 \cdot 10^{19}$	$5.14 \cdot 10^{18}$
23	$-1.07 \cdot 10^{19}$	$-1.24 \cdot 10^{19}$	—
24	—	—	$3.09 \cdot 10^{17}$
25	$2.28 \cdot 10^{17}$	$4.17 \cdot 10^{18}$	$4.96 \cdot 10^{18}$
33	$2.08 \cdot 10^{18}$	$2.45 \cdot 10^{18}$	—
34	—	—	—
35	$-2.06 \cdot 10^{15}$	$9.60 \cdot 10^{15}$	—
44	—	—	$1.20 \cdot 10^{17}$
45	—	—	$1.49 \cdot 10^{17}$
55	$5.48 \cdot 10^{16}$	$1.02 \cdot 10^{18}$	$1.21 \cdot 10^{18}$

TABLE XI: Normalization factors for $\Delta\Phi_{jj}$ distributions in $H+2\text{-jets}$ production induced by higher dimensional operators for a scalar Higgs (see fig. 12).

σ_{ij}/pb for $H+2\text{-jet}$ (pseudo-scalar), WBF cuts			
ij	gg	gq	qq
22	$1.40 \cdot 10^{19}$	$2.01 \cdot 10^{19}$	$4.88 \cdot 10^{18}$
23	$-1.07 \cdot 10^{19}$	$-1.24 \cdot 10^{19}$	—
24	—	—	—
25	$2.28 \cdot 10^{17}$	$4.12 \cdot 10^{18}$	$4.71 \cdot 10^{18}$
33	$2.26 \cdot 10^{15}$	$2.45 \cdot 10^{18}$	—
34	—	—	—
35	$-2.06 \cdot 10^{15}$	$9.62 \cdot 10^{15}$	—
44	—	—	—
45	—	—	—
55	$5.49 \cdot 10^{16}$	$1.01 \cdot 10^{18}$	$1.15 \cdot 10^{18}$

TABLE XII: Same as table XI, but for a pseudo-scalar Higgs (see fig. 13).

σ_{ij}/pb for $H+2\text{-jet}$ (scalar), incl. cuts			
ij	gg	gq	qq
22	$7.10 \cdot 10^{20}$	$3.10 \cdot 10^{20}$	$9.56 \cdot 10^{19}$
23	$-5.62 \cdot 10^{20}$	$-1.36 \cdot 10^{20}$	—
24	—	—	$1.69 \cdot 10^{19}$
25	$4.21 \cdot 10^{18}$	$1.38 \cdot 10^{20}$	$9.38 \cdot 10^{19}$
33	$1.12 \cdot 10^{20}$	$2.86 \cdot 10^{19}$	—
34	—	—	—
35	$-4.94 \cdot 10^{17}$	$1.65 \cdot 10^{18}$	—
44	—	—	$4.26 \cdot 10^{18}$
45	—	—	$8.37 \cdot 10^{18}$
55	$7.18 \cdot 10^{17}$	$3.49 \cdot 10^{19}$	$2.32 \cdot 10^{19}$

TABLE XIII: Normalization factors for $\Delta\eta_{jj}$ distributions in $H+2\text{-jets}$ production induced by higher dimensional operators for a scalar Higgs (see fig. 14).

σ_{ij}/pb for $H+2\text{-jet}$ (pseudo-scalar), incl. cuts			
ij	gg	gq	qq
22	$7.11 \cdot 10^{20}$	$3.10 \cdot 10^{20}$	$8.33 \cdot 10^{19}$
23	$-5.62 \cdot 10^{20}$	$-1.37 \cdot 10^{20}$	—
24	—	—	—
25	$4.19 \cdot 10^{18}$	$1.39 \cdot 10^{20}$	$8.15 \cdot 10^{19}$
33	$5.12 \cdot 10^{18}$	$2.86 \cdot 10^{19}$	—
34	—	—	—
35	$-4.94 \cdot 10^{17}$	$1.65 \cdot 10^{18}$	—
44	—	—	—
45	—	—	—
55	$7.15 \cdot 10^{17}$	$3.50 \cdot 10^{19}$	$2.01 \cdot 10^{19}$

TABLE XIV: Same as table XIII, but for a pseudo-scalar Higgs (see fig. 15).

-
- [1] G. Aad *et al.* [ATLAS Collaboration], *Observation of a new particle in the search for the Standard Model Higgs boson with the ATLAS detector at the LHC*, *Phys. Lett. B* **716** (2012) 1, [arXiv:1207.7214](#).
 - [2] S. Chatrchyan *et al.* [CMS Collaboration], *Observation of a new boson at a mass of 125 GeV with the CMS experiment at the LHC*, *Phys. Lett. B* **716** (2012) 30, [arXiv:1207.7235](#).
 - [3] The LHC Higgs Cross Section Working Group Collaboration, *Handbook of LHC Higgs Cross Sections: 3. Higgs Properties*, [arXiv:1307.1347](#).
 - [4] S. Dittmaier *et al.* [LHC Higgs Cross Section Working Group Collaboration], *Handbook of LHC Higgs cross sections: 2. differential distributions*, [arXiv:1201.3084](#).
 - [5] S. Dittmaier *et al.* [LHC Higgs Cross Section Working Group Collaboration], *Handbook of LHC Higgs cross sections: 1. inclusive observables*, [arXiv:1101.0593](#).
 - [6] LHC Higgs Cross Section Working Group, *LHC HXSWG interim recommendations to explore the coupling structure of a Higgs-like particle*, [arXiv:1209.0040](#).
 - [7] G. F. Giudice, C. Grojean, A. Pomarol and R. Rattazzi, *The Strongly-Interacting Light Higgs*, *JHEP* **0706** (2007) 045, [[hep-ph/0703164](#)].
 - [8] G. Passarino, *NLO Inspired Effective Lagrangians for Higgs Physics*, *Nucl. Phys. B* **868** (2013) 416, [arXiv:1209.5538](#).
 - [9] V. Hankele, G. Klamke, D. Zeppenfeld, T. Figy, *Anomalous Higgs boson couplings in vector boson fusion at the CERN LHC*, *Phys. Rev. D* **74** (2006) 095001, [[hep-ph/0609075](#)].
 - [10] U. Langenegger, M. Spira, A. Starodumov, P. Trueb, *SM and MSSM Higgs Boson Production: Spectra at large transverse Momentum*, *JHEP* **0606** (2006) 035, [[hep-ph/0604156](#)].
 - [11] F. Campanario, M. Kubocz, D. Zeppenfeld, *Gluon-fusion contributions to $\Phi + 2$ Jet production*, *Phys. Rev. D* **84** (2011) 095025, [arXiv:1011.3819](#).
 - [12] E. Bagnaschi, G. Degrossi, P. Slavich, A. Vicini, *Higgs production via gluon fusion in the POWHEG approach in the SM and in the MSSM*, *JHEP* **1202** (2012) 088, [arXiv:1111.2854](#).
 - [13] J.A. Gracey, *Classification and one loop renormalization of dimension-six and dimension-eight operators in quantum gluodynamics*, *Nucl. Phys. B* **634** (2002) 192; erratum *ibid.* **696** (2004) 295, [[hep-ph/0204266](#)].
 - [14] D. Neill, *Two-Loop Matching onto Dimension Eight Operators in the Higgs-Gluon Sector*, [arXiv:0908.1573](#).
 - [15] J. Germer, *Maximally Helicity Violating amplitudes for Higgs production processes*, Diploma thesis (supervisor: D. Zeppenfeld), Universitat Karlsruhe (2007), http://www.itp.kit.edu/prep/diploma/PSFiles/Diplom_Germer.pdf.
 - [16] K.G. Chetyrkin, J.H. Kuhn, C. Sturm, *QCD decoupling at four loops*, *Nucl. Phys. B* **744** (2006) 121, [[hep-ph/0512060](#)].
 - [17] Y. Schroder and M. Steinhauser, *Four-loop decoupling relations for the strong coupling*, *JHEP* **0601** (2006) 051, [[hep-ph/0512058](#)].
 - [18] C. Arzt, *Reduced effective Lagrangians*, *Phys. Lett. B* **342** (1995) 189, [[hep-ph/9304230](#)].
 - [19] H. Georgi, *On-shell effective field theory*, *Nucl. Phys. B* **361** (1991) 339.
 - [20] H. D. Politzer, *Power Corrections at Short Distances*, *Nucl. Phys. B* **172** (1980) 349.
 - [21] A. Semenov, *LanHEP: A Package for the automatic generation of Feynman rules in field theory. Version 3.0*, *Comp. Phys. Commun.* **180** (2009) 431, [arXiv:0805.0555](#).
 - [22] N.D. Christensen and C. Duhr, *FeynRules - Feynman rules made easy*, *Comp. Phys. Commun.* **180** (2009) 1614, [arXiv:0806.4194](#).
 - [23] M. Tentyukov and J. Fleischer, *A Feynman diagram analyzer DIANA*, *Comp. Phys. Commun.* **132** (2000) 124, [[hep-ph/9904258](#)].
 - [24] J.A. Vermaseren, *New features of FORM*, [[math-ph/0010025](#)].
 - [25] R.V. Harlander, S. Liebler and H. Mantler, *SusHi: A program for the calculation of Higgs production in gluon fusion and bottom-quark annihilation in the Standard Model and the MSSM*, *Comp. Phys. Commun.* **184** (2013) 1605, [arXiv:1212.3249](#).
 - [26] R.V. Harlander, T. Neumann, K.J. Ozeren, M. Wiesemann, *Top-mass effects in differential Higgs production through gluon fusion at order α_s^4* , *JHEP* **1208** (2012) 139, [arXiv:1206.0157](#).
 - [27] V. Del Duca, W. Kilgore, C. Oleari, C.R. Schmidt, D. Zeppenfeld, *Kinematical limits on Higgs boson production via gluon fusion in association with jets*, *Phys. Rev. D* **67** (2003) 073003, [[hep-ph/0301013](#)].
 - [28] V. Del Duca, W. Kilgore, C. Oleari, C. Schmidt, D. Zeppenfeld, *Gluon-fusion contributions to $H + 2$ jet production*, *Nucl. Phys. B* **616** (2001) 367, [[hep-ph/0108030](#)].
 - [29] D.L. Rainwater and D. Zeppenfeld, *Searching for $H \rightarrow \gamma\gamma$ in weak boson fusion at the LHC*, *JHEP* **9712** (1997) 005, [[hep-ph/9712271](#)].
 - [30] G. Klamke and D. Zeppenfeld, *Higgs plus two jet production via gluon fusion as a signal at the CERN LHC*, *JHEP* **0704** (2007) 052, [[hep-ph/0703202](#)].
 - [31] V. Hankele, G. Klamke and D. Zeppenfeld, *Higgs + 2 jets as a probe for CP properties*, [[hep-ph/0605117](#)].
 - [32] K. Arnold *et al.*, *Release Note – vbfNLO-2.6.0*, [arXiv:1207.4975](#).
 - [33] K. Arnold *et al.*, *VBFNLO: A Parton Level Monte Carlo for Processes with Electroweak Bosons – Manual for Version 2.5.0*, [arXiv:1107.4038](#).
 - [34] K. Arnold *et al.*, *VBFNLO: A parton level Monte Carlo for processes with electroweak bosons*, *Comp. Phys. Commun.* **180** (2009) 1661, [arXiv:0811.4559](#).